Separation Science and Technology
Publication details, including instructions for authors and subscription information:
http://www.informaworld.com/smpp/title~content=t713708471

3-D Simulation of Electroosmotic Injection and Migration in Microchannels: Effects of Non-Rectangular Cross Section

Doh-Hyoung Lee[a]; Bakhtier Farouk[a]; H. -S. Noh[a]
[a] Mechanical Engineering and Mechanics Department, Drexel University, Philadelphia, PA, USA

Online publication date: 18 January 2011

To cite this Article Lee, Doh-Hyoung , Farouk, Bakhtier and Noh, H. -S.(2011) '3-D Simulation of Electroosmotic Injection and Migration in Microchannels: Effects of Non-Rectangular Cross Section', Separation Science and Technology, 46: 2, 195 — 204
To link to this Article: DOI: 10.1080/01496395.2010.519369
URL: http://dx.doi.org/10.1080/01496395.2010.519369

Separation Science and Technology, 46: 195–204, 2011

ISSN: 0149-6395 print/1520-5754 online
DOI: 10.1080/01496395.2010.519369

Taylor & Francis
Taylor & Francis Group

3-D Simulation of Electroosmotic Injection and Migration in Microchannels: Effects of Non-Rectangular Cross Section

Doh-Hyoung Lee, Bakhtier Farouk, and H.-S. Noh
Mechanical Engineering and Mechanics Department, Drexel University, Philadelphia, PA, USA

A numerical study of the 3-D characteristics of electroosmotic injection and migration of sample species in microchip capillary electrophoresis systems is reported. In particular, the effect of a non-rectangular cross section commonly found in isotropically-etched microchannels is thoroughly investigated through 3-D numerical simulations. A non-rectangular cross section resulted in a vertically non-uniform sample plug during the loading stage. Conventional 2-D simulation approach can result in up to 40% errors in the calculation of injection qualities. It was also found that the 2-D simulation using a proper channel width has a good agreement with the 3-D simulation data.

Abbreviations EDL, electric double layer; DC, direct current; 3-D, three-dimensional

Keywords DC electrokinetics; electroosmosis; 3-D simulation; microchip capillary electrophoresis; pinched injection

INTRODUCTION

Electroosmosis is the motion of liquid induced by an applied electric field along a capillary tube or microchannel. This bulk fluid flow is due to the migration of ions collected near the channel surface in the form of an electrical double layer (EDL) (1). The EDL thickness in typical operating liquid media ranges only up to a few nanometers (2–4) from the channel wall, which is much smaller than the cross-sectional dimensions of typical microchannels. The thinness of the electric double layer makes the induced bulk flow behave like a wall-driven flow that has a uniform velocity profile (4). The uniform velocity profile makes the electroosmotic flow very attractive in separation science because dynamic dispersion and band broadening effects can be minimized with such a velocity profile, compared to the parabolic velocity profile of pressure-driven flows.

Received 19 March 2010; accepted 25 August 2010.
Submitted for publication, *Separation Science and Technology*, March 2010.
Address correspondence to Professor H.-S. Noh, Mechanical Engineering and Mechanics Department, Drexel University, 3141 Chestnut Street, Room 2-115, Philadelphia, PA 19104, USA. Tel.: +1-215-895-2273; Fax: +1-215-895-1478. E-mail: mosesnoh@coe.drexel.edu

The thin velocity boundary layer and the consequent uniform velocity profile of electroosmotic flow has also served as the basis for many previous numerical simulation studies, which employed a 2-D (4–8) or even an 1-D (9–11) approximation. The lower dimensional (1-D or 2-D) approximation is valid if there is no variation in any critical parameters in the eliminated dimensions. 1-D approximation has been usually considered for the simulation of traditional capillary electrophoresis systems (single channel systems) while 2-D approximation has been used for the simulation of multiple branch microchannel electrophoresis systems such as a pinched injection system. This paper focuses on the evaluation of 2-D approximation for the simulation of pinched injection systems. 2-D and 3-D simulations have been performed and carefully compared to elucidate the significance of considering 3-D characteristics.

Most previous simulation studies (4–8) on pinched injection systems were based on 2-D simulation. Ermakov et al. simulated the sample concentration distribution during the focusing and dispensing stages of a pinched injection by applying the Helmholtz-Smoluchowski slip velocity condition on a 2-D computational domain to find the optimal operation conditions (4,6). Fu et al. compared their experiments on the performance of capillary electrophoresis microchips with 2-D simulations (7–8). Patankar and Hu used a 3-D rectangular channel geometry (12). However, the emphasis of the study was for investigating the effect of external pressure gradients on the sample focusing behavior. To the best of our knowledge, no previous paper has investigated the 3-D characteristics of the electroosmotic pinched injection and quantitatively discussed the significance of 3-D simulation.

For channels with rectangular cross-sections, a 2-D approximation is sufficient because the similitude between electroosmotic flow and electric field solutions (13) guarantees no variation of any parameters in the vertical direction. This is because, if the similitude is assured, the flow profile along the top wall of a rectangular 3-D case will be the same as the flow in the 2-D case. However, in real capillary electrophoresis microchips most microchannels are made preferentially out of glass substrates via isotropic wet

etching process (7–8,14–15), resulting in a highly non-rectangular cross section. The curved surface of an isotropically-etched microchannel will distort the pinched sample plug although each channel branch still has a uniform velocity profile. This paper investigates how the non-rectangular 3-D geometries of a channel affect loading and dispensing of a sample species during pinched injection and provides a quantitative assessment of 2-D approximations compared to accurate 3-D simulation data.

PROBLEMS CONSIDERED

Sample Loading

The 3-D characteristics of sample loading in a pinched injection system are investigated by using a non-rectangular, isotropically-etched microchannel as shown in Fig. 1(a). This model geometry represents glass microchannels commonly made by wet etching techniques. The channel is 50 μm wide at the top (W_t), 90 μm wide at the bottom (W_b), and 20 μm high (H). In order to save computational time and memory, only the region around the intersection, instead of the entire microchannel system, is used as a computational domain ($L_s = L_w = L_b = 300\,\mu m$ and $L_c = 1000\,\mu m$). Both narrow and wide sample plugs can be produced by controlling the three inlet flows via applied electric fields. The electric field conditions used for sample loading methods are specified in Table 1. The subscripts, s, w, b, and c, denote the sample, waste, buffer, and collect channels respectively. The cross-sectional distribution of the sample species at the intersection was carefully investigated using 3-D simulations. Particularly, the vertical non-uniformity induced by the non-rectangular 3-D channel geometry was investigated.

Sample Dispensing

The 3-D characteristics of sample dispensing of the pinched injection were investigated for various cross-sectional geometries as shown in Fig. 1(b). 3-D geometries include an isotropically-etched cross section and a trapezoidal cross section. For 2-D simulation, several different channel widths were selected for comparison. Note that the channel width used in previous 2-D simulation studies were the top width (W_t) or bottom width (W_b) or average width of the channel ($(W_t + W_b)/2$). We considered one more channel width that is calculated from the equivalent cross-sectional area and height of the isotropically-etched cross section, i.e., $W = (\pi H^2/2 + W_t\ H)/H$. The narrow sample loading method (Table 1) was selected as the initial condition. The dispensing electric fields were selected to have maximum injection efficiency based on the Ermakov's report (6).

TABLE 1
Electric field values at the inlets and outlets for loading and dispensing stages (Loading *Method 1*: narrow loading, *Method 2*: wide loading)

	Loading		
	Method 1	*Method 2*	Dispensing
E_s	3 kV/m	30 kV/m	−10 kV/m
E_b	10 kV/m	10 kV/m	30 kV/m
E_c	10 kV/m	10 kV/m	−10 kV/m
E_w	−23 kV/m	−50 kV/m	−10 kV/m

Sample Migration

The effect of 3-D non-rectangular geometry on sample dispersion during electroosmotic migration was also investigated. Since the electroosmotic flow and electrophoretic sample motion are both uniform, they do not affect the dispersion of a sample plug if there is no pressure gradient in the channel. In other words, the dispersion of a sample plug during electroosmotic migration in a straight channel

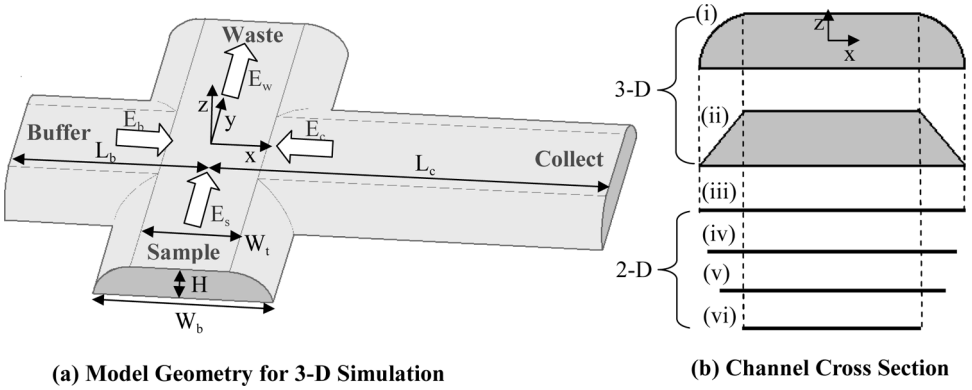

FIG. 1. A schematic geometry of the 3-D computational domain. (a) Definition of dimensional and operational parameters, and (b) 6 different channel cross sections investigated for the sample dispensing study; i) isotropically-etched cross section (3-D), ii) trapezoidal cross section (3-D), iii-vi) 2-D geometries with various widths (iii: 90 μm (W_b), iv: 81.4 μm (A/H where A is the cross-sectional area of the isotropically etched channel), v: 70 μm ($(W_b+W_t)/2$), vi: 50 μm (W_t)).

is determined only by the molecular diffusion. If the sample plug has no variation in the lateral direction, the problem further simplifies to a trivial 1-D diffusion case and there would be no difference between 3-D and lower dimensional simulations. However, in reality, the sample plug is not laterally uniform but close to a triangular shape after a pinched injection. 2-D simulation would be sufficient if the channel is rectangular and the concentration profile is constant in z-direction. But for channels with non-rectangular geometry the lateral dispersion of a sample plug will be further perturbed due to the concentration gradient in z-direction developed during sample migration. In order to study this effect, we selected a simple triangular sample plug as initial condition and performed 2-D and 3-D simulations. The model geometries selected for this study are a 2-D channel with a width of 90 μm and a 3-D isotropically-etched channel ($W_b = 90\,\mu m$ and $H = 20\,\mu m$). The effect of non-rectangular channel geometry on the band broadening was investigated using 3-D simulations.

GOVERNING EQUATIONS

The general governing equation for the dynamics of electroosmotic flow is derived by adding the electric body force to the incompressible Navier-Stokes equation and the momentum equation is solved together with the electric potential developed from the ionic distribution in an electric double layer (12). Since the thin Debye length approximation is employed in this study, the flow problem can be further simplified to a slip velocity problem with the Helmholtz-Smoluchowski electroosmotic velocity (1,4). This approximation is well accepted and saves significant computational time and memory by avoiding very fine meshes near the wall for capturing the velocity profile within the electric double layer. Detailed validation and explanation of the Helmholtz-Smoluchowski electroosmotic slip velocity is described in references (1,4). The governing equations for the current problem are as follows:

$$\text{Flow continuity equation: } \nabla \cdot \vec{V} = 0 \tag{1}$$

$$\text{Flow momentum equation: } \rho \frac{D\vec{V}}{Dt} = -\nabla p + \eta \nabla^2 \vec{V} \tag{2}$$

$$\text{Helmholtz-Smoluchowski slip velocity: } \vec{V}_{eo} = \mu_{eo}\vec{E} \tag{3}$$

$$\text{Electric potential governing equation: } \nabla^2 \Phi = 0 \tag{4}$$

$$\text{Chemical species conservation: } \frac{\partial C}{\partial t} + \nabla \cdot ((\vec{V} + \mu_{ep}\vec{E})C) = D\nabla^2 C \tag{5}$$

where $\vec{V}$ is flow velocity, ρ is the density, η is the dynamic viscosity, $\vec{E}$ is the applied electric field, C is sample species concentration, D is the diffusivity of sample species, and μ_{eo} and μ_{ep} are the electroosmotic and electrophoretic mobilities. The complete form of electric potential equation contains the effect of conductivity variation and ion densities. A simpler form, Eq. (4), was derived by assuming a constant conductivity and negligible effect of ion distribution on the activation electric field (12). The governing equation of sample concentration, Eq. (5), is a linear equation in terms of the sample concentration, and the sample concentration does not influence other parameters such as $\vec{V}$ or Φ in this simulation. All sample concentration results here are normalized by the sample concentration delivered from the sample reservoir (C_0), denoted by C^*.

SIMULATION METHOD

COMSOL multiphysics version 3.5a was used for the simulations in this study. The general parameter values for the current simulations are the electroosmotic mobility $(\mu_{eo}) = 4 \times 10^{-8}\,m^2/Vs$, the electrophoretic mobility of sample $(\mu_{ep}) = -1 \times 10^{-8}\,m^2/Vs$, the diffusivity of sample $(D) = 1 \times 10^{-10}\,m^2/s$, the solution density $(\rho) = 1000\,kg/m^3$, the dynamic viscosity of solution $(\eta) = 0.001\,kg/m\,s$. The selected electroosmotic mobility corresponds to a ζ-potential of about 60 mV, which is a typical value for glass or other polymer substrates in standard conditions (16). This value was also used in previous papers (4,17). The selected diffusivity and electrophoretic mobility values match typical values for small proteins or large fluorescent dyes (18–19). The COMSOL software has formulated modules for various physics equations in the name of application modes. We selected three application modes from the COMSOL software, *Conductive Media DC* (for electric potential, Eq. (4)), *Incompressible Navier-Stokes* (for fluid flow, Eqs. (1) and (2)), and *Electrokinetic Flow* (for species concentration, Eq. (5)), for the simulations in this study. At the walls, insulation boundary conditions ($\partial\Phi/\partial n = 0$, $\partial C/\partial n = 0$) were imposed for the electric potential and chemical species simulations while the Helmholtz-Smoluchowski slip velocity (Eq. (3)) was imposed for the flow simulation as the wall boundary condition. The zero pressure boundary condition was imposed at the inlets and outlets, based on the fact that there is no pressure difference between each individual inlet and outlet reservoir and the assumption that pressure gradient along each channel is negligible. This zero pressure boundary condition (also known as the periodic boundary condition) has been adopted in some previous reports (12,17,20) while others (21–22) used the zero pressure gradient boundary condition. We found that there is no more than a 0.2% difference in the velocity field solutions obtained using the two different pressure boundary conditions. The outlet condition for the species conservation (Electrokinetic Flow) assumes that the mass flow through the boundary is dominated by convection. This condition has often been adopted in previous reports (22–23).

For the simulation of a pinched injection, the loading stage solution is calculated first by using steady-state computation for all three computation modes in the sequence of *Conductive Media DC, Incompressible Navier-Stokes* and *Electrokinetic Flow* modes. The solution of sample concentration at the loading stage is then used as an initial condition for the dispensing stage sample concentration, which is solved with a time-dependent solver. Even for the dispensing stage, the *Conductive Media DC* and *Incompressible Navier-Stokes* equations are solved in steady-state computation, while the *Electrokinetic Flow* equation is solved with time-dependent calculation ($0 \sim 3$ sec).

We have observed significant numerical errors when sharp corners exist in the microchannel geometry even with extremely fine mesh around the corners (The numerical inaccuracy will be discussed in the Results and Discussion section). A 1-μm radius fillet was applied on the corners for 2-D cases for an accurate simulation. The small fillets applied to the corners did not significantly change the performance of the device, and they relieved the numerical inaccuracy related with the sharp corners.

RESULTS AND DISCUSSION

Model Validation

The current simulation method was first validated by comparing the predictions with previous numerical (4) and experimental (24) data. The channel geometry selected for the present 3-D simulation is an isotropically-etched microchannel with a bottom width of 24 μm and a height of 6.4 μm as described in (24). The geometry for the 2-D simulation was the same as the previous simulation described in (4) (channel width = 24 μm) except for having the fillet of radius 0.1 μm at the intersection corners. Figure 2 compares the normalized sample concentration profiles at 3 μm upstream ($y = -15$ μm) from the intersection obtained by 2-D and 3-D simulations with experimental data that is an accumulated sample concentration from the top view along the x-axis. The graph shows that the 3-D simulation result has a better agreement with the experimental data compared to the previous and current 2-D simulation results. This result supports that our 3-D simulation model is valid and accurate.

3-D Characteristics in Sample Loading

Figures 3 and 4 show the top and cross-sectional views of the sample concentration profile during sample loading in pinched injection in an isotropically-etched microchannel. The top view represents the sample concentration distribution on the top boundary surface of the 3-D channel geometry, while the cross-sectional views (x-z plane) show the vertical (in z direction) variation in the concentration profile. The narrow loading method (Table 1) resulted in a V-shaped concentration profile in the z direction while the broad loading method produced a Λ-shaped concentration profile. In the narrow sample loading, the flows from the buffer and collect channels are higher than the flow from the sample channel so that the sample band becomes narrow and focused at the intersection. This flow is not uniform in

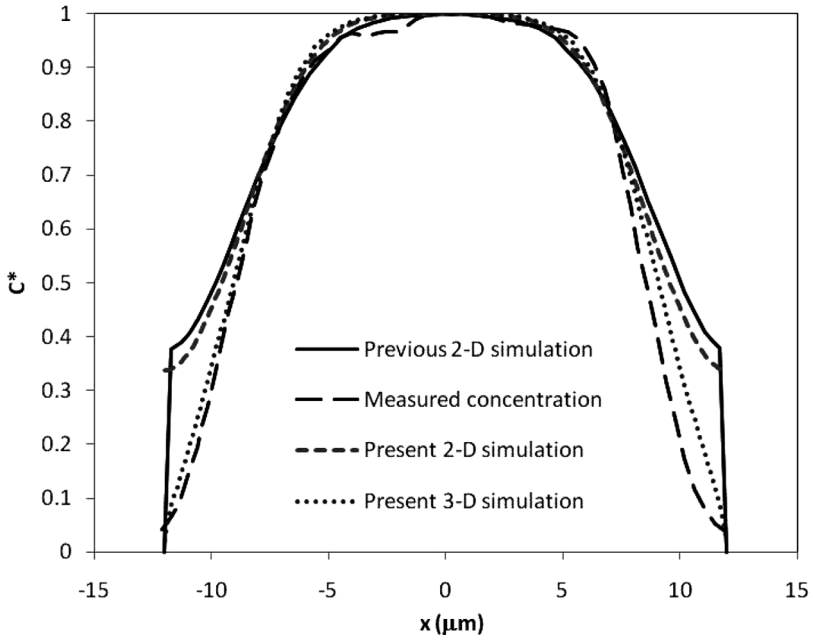

FIG. 2. Normalized sample concentration profile at 3 μm upstream from the focusing chamber for the present 2-D and 3-D simulations compared with previous 2-D numerical (4) and experimental (24) data.

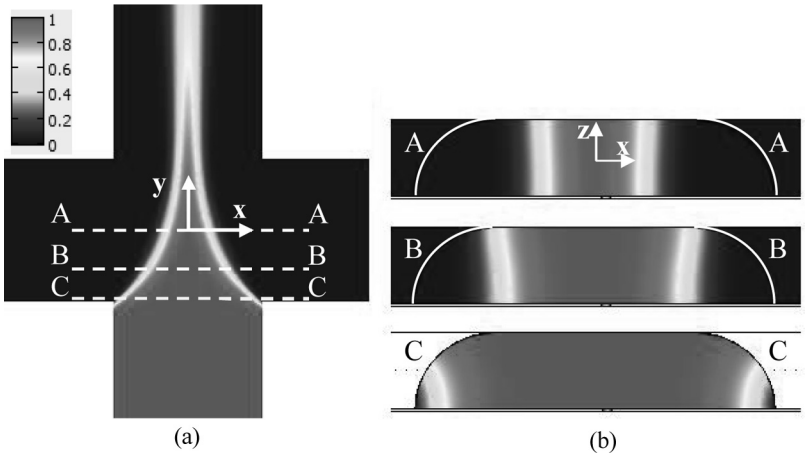

FIG. 3. Normalized sample concentration distribution during a narrow sample loading in an isotropically-etched microchannel. (a) Top view and (b) cross-sectional views (A-A: $y = 0$, B-B: $y = -25\,\mu m$, and C-C: $y = -45\,\mu m$).

the vertical coordinate because of the curved top surface near the corners at the intersection. The lower part of the sample plug ($z < 0$) encounters the strong narrowing flows from the buffer and collect channels first before the upper part does at the intersection because of the isotropically-etched geometry. Therefore the lower part is compressed more than the upper part resulting in a V-shape sample band. In the case of wide sample loading, the opposite motion occurs. The flows from the buffer and collect channels are lower than that of the sample channel so the sample band becomes wide at the intersection. Now the opposite expanding action is strong in the lower part of the sample plug ($z < 0$), resulting in a Λ-shape sample plug.

Figure 5 shows the distribution of the vertical (z-directional) component of flow velocity, w, in a 3-D isotropically-etched channel geometry. In a rectangular microchannel, the vertical velocity component is always zero. However, in a non-rectangular microchannel, the vertical velocity component arises due to the 3-D characteristic of the geometry as shown in Fig. 5. The vertical velocity component is strong near the corners of channel intersection, where the flow is guided up and down by the curved top surface. The three solid curves (L_1, L_2, and L_3) in Fig. 5 represent flow streamlines passing through the corners of the intersection. The streamline falls down when it passes the negative w region, and it rises when it passes the positive w region. The maximum elevation along L_2 was 3.4 μm, which is 17% of the channel height.

3-D Characteristics in Sample Dispensing

For a quantitative and proper comparison between 2-D and 3-D simulation results, the averaged sample concentration data as a function of x (the axis along the migration channel) were obtained by the following equations:

$$C^*_{average}(x) = \frac{\int\int C(x,y,z)dydz}{C_0 A} \text{ for 3-D and}$$
$$C^*_{average}(x) = \frac{\int C(x,y)dy}{C_0 W} \text{ for 2-D} \quad (6)$$

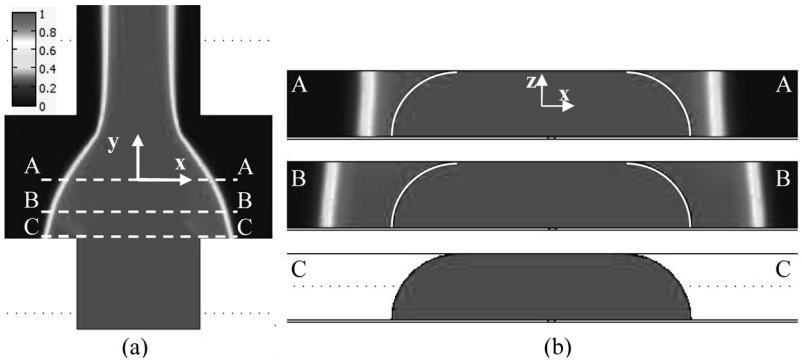

FIG. 4. Normalized sample concentration distribution during a wide sample loading in an isotropically-etched microchannel. (a) Top view and (b) cross-sectional views (A-A: $y = 0$, B-B: $y = -25\,\mu m$, and C-C: $y = -45\,\mu m$).

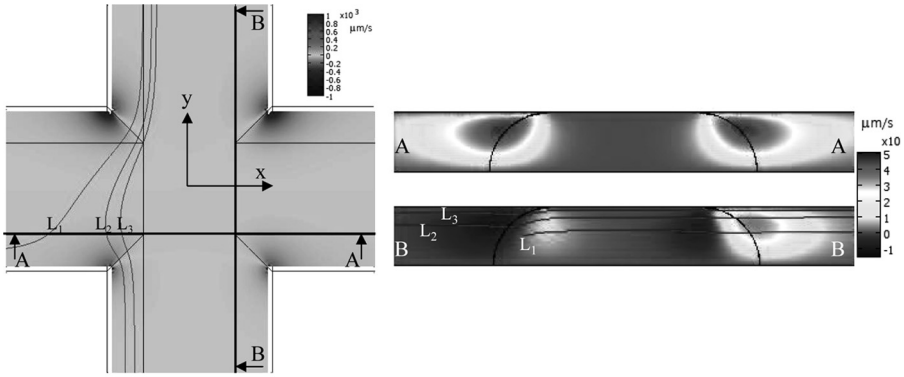

(a) (b)

FIG. 5. The variation of vertical velocity component (w) in an isotropically-etched channel for a wide sample loading case. (a) Vertical velocity distribution at the $z = 0$ plane and (b) cross-sectional views (along A-A: $x = 25\,\mu m$ and along B-B: $y = -25\,\mu m$). Solid lines are streamlines passing through the corners of the intersection at different locations: ($-200\,\mu m$, $-35\,\mu m$, $0\,\mu m$) for L_1, ($-35\,\mu m$, $-200\,\mu m$, $-4\,\mu m$) for L_2 and ($-30\,\mu m$, $-200\,\mu m$, $8\,\mu m$) for L_3.

where A is the cross-sectional area of 3-D channel and W is the cross width of 2-D channel. This averaged concentration along x-axis corresponds to the signal from a detector commonly used in capillary electrophoresis, such as laser induced fluorescence (LIF).

Figure 6 shows the averaged concentration distribution at different traveling times ($t = 0$, 1, and 2 sec) and the variation of peak value with traveling distance (x) for 2-D and 3-D simulations. Since the concentration data were averaged across the transverse cross section (y-z plane), the band width (σ) of the sample concentration profile did not have significant variation among the 3-D and 2-D simulation data at different times. However, there was quite a significant difference in the peak value of the concentration profile and its variation with the traveling distance. The 3-D simulation data for the isotropically-etched cross section lies between two cases of 2-D simulation data ($W = 90\,\mu m$ and $W = 70\,\mu m$) while the 3-D simulation data for a trapezoidal cross section lies between the $W = 90\,\mu m$ and $W = 50\,\mu m$ cases. The percent differences of 2-D peak concentrations for the cases of $W = 90\,\mu m$, $81.4\,\mu m$, $70\,\mu m$, and $50\,\mu m$ from the 3-D simulation value (isotropically-etched cross section) at $t = 2$ sec are 5.86%, −2.28%, −12.93% and −34.99%, respectively. The 3-D simulation data for the isotropically etched cross section and the trapezoidal cross section were close to the 2-D simulation data of $W = 81.4\,\mu m$ (2.28% difference) and $W = 70\,\mu m$ (2.66% difference), respectively. This observation shows that selection of the channel width is very important in the simplified 2-D simulation approach. The

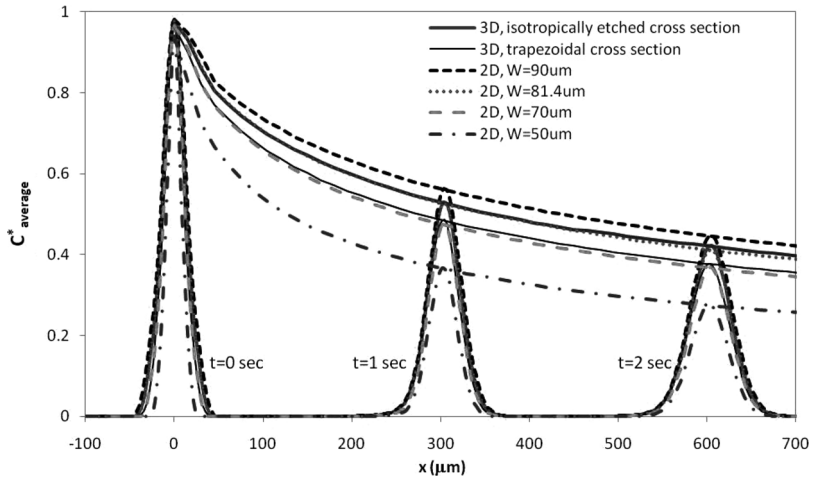

FIG. 6. The averaged sample concentration distribution at different traveling times ($t = 0$, 1, and 2 sec) and the variation of peak value with traveling distance (x) calculated from 3-D and 2-D simulation data. A narrow sample loading was used. Sample concentration was normalized by the initial sample concentration value.

channel width equivalent to the width of the rectangular cross section having the same height and cross sectional area as the 3-D cross section produces more accurate average concentration distributions.

A normalized injected sample amount can be represented by the area under the averaged concentration curve in Fig. 6. Equation (7) shows how the normalized injected sample amount is calculated for 2-D and 3-D simulation data. Since the injected sample amount was normalized by the cross-sectional area (for 3-D) or width (for 2-D), this parameter has a unit of the length, instead of the volume. This definition is used for a proper comparison between 2-D and 3-D simulation data.

$$\begin{aligned} \textit{Normalized injected sample amount} &= \int C^{*}_{average}(x)dx \\ &= \frac{\int\int\int C(x,y,z)dydzdx}{C_0 A} = \frac{\textit{Injected sample volume}}{A} \\ \text{for 3-D and } \int C^{*}_{average}(x)dx &= \frac{\int\int C(x,y)dydx}{C_0 W} \\ &= \frac{\textit{Injected sample area}}{W} \text{ for 2-D} \end{aligned} \tag{7}$$

The normalized injected sample amounts in 3-D simulation for the cases of the isotropically-etched cross section and the trapezoidal cross section were 24.2 μm and 21.7 μm, respectively. The values in 2-D simulation for the cases of W = 90 μm, 81.4 μm, 70 μm and 50 μm were 26.6 μm, 24.1 μm, 20.7 μm, and 14.7 μm, respectively. Considering that there is no significant difference in the sample band width between 2-D and 3-D simulation data, the difference in peak values shown in Fig. 6 can be attributed to the different injected sample amount between 2-D and 3-D cases. Again, the injected sample amount for 3-D geometry with the isotropically-etched cross section is similar to the 2-D case with W = 81.4 μm. The percent differences of 2-D simulation injected amounts for the cases of W = 90 μm, 81.4 μm, 70 μm, and 50 μm from the 3-D value are 9.77%, −0.78%, −14.77% and −39.27%, respectively. We have also calculated the injection characteristic of a pinched injection system (6), C_{peak}/σ where C_{peak} is the peak value of a sample concentration distribution and σ is the spatial standard deviation along the x coordinate defined by $\sigma = \sqrt{\int C(x)(x-X)^2dx / \int C(x)dx}$ and $X = \int C(x)xdx / \int C(x)dx$ (data not shown). The results were similar to the averaged concentration profile results and normalized injected sample amount results. Up to 40% differences were observed between 2-D and 3-D simulation results but 2-D simulation with the channel width equivalent to the width of the rectangular cross section having the same height and cross sectional area as the 3-D cross section showed only 2% difference from 3-D data.

One further question is how the effect of 3-D geometry (isotropically-etched profile) of a microchannel on injection qualities will change as the channel aspect ratio (H/W_b) is varied. Figure 7 shows the effect of channel height on the 3-D simulation results for the isotropically-etched cross section case, compared with the large width 2-D case. For the isotropically-etched cross sectional channel, the radius of the curved area is equal to the height and the bottom channel width is fixed to 90 μm. Thus, as the channel height decreases, the region of the curved top surface decreases. With decreasing channel height, the 3-D characteristics also decrease and the 3-D results approach the 2-D results.

3-D Characteristics of Sample Dispersion during Migration in a Straight Migration Channel

The 3-D characteristics of a sample dispersion during migration were investigated by simulating the molecular diffusion of an initially triangular sample plug in a straight channel. Figure 8 shows the variation of the averaged

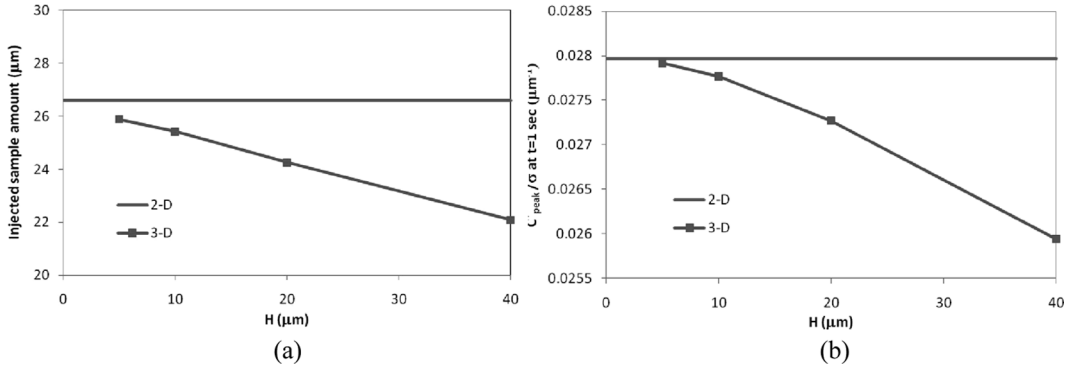

FIG. 7. The effect of channel height on the 3-D injection performances compared to 2-D results. (a) Sample injection amount and (b) injection characteristic. 2-D channel width = 90 μm (blue line). For the isotropically-etched cross-sectional channel, the radius of the curved area is equal to the height of the channel. The bottom channel width was fixed at 90 μm while the height (H) was varied. With decreasing channel height, the 3-D characteristics also decrease and the 3-D results approach to the 2-D results.

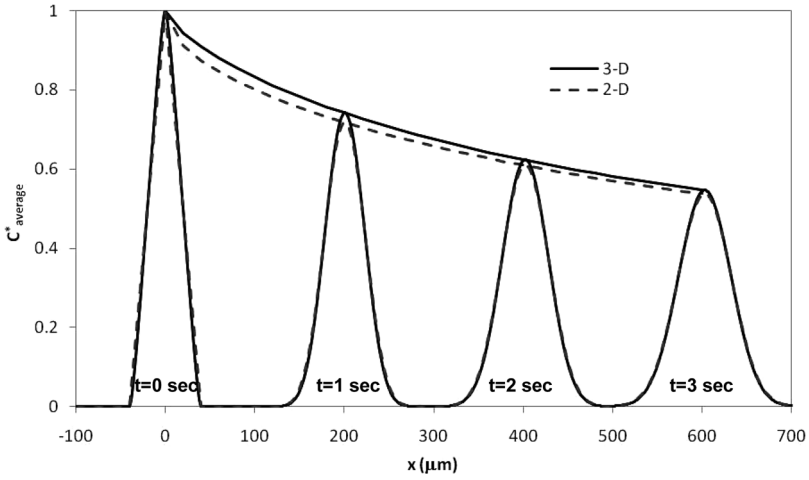

FIG. 8. The averaged sample concentration distribution at different traveling times (t = 0, 1, 2, and 3 sec) and the variation of peak value with traveling distance (x) calculated from 3-D and 2-D simulation data for sample migration case. The shape of the initial sample plug is triangular. The migration speed is 200 μm/sec.

sample concentration distribution in a 2-D channel with W = 90 μm and in a 3-D isotropically-etched channel as the sample travels with the speed of 200 μm/s (The traveling velocity is arbitrarily specified. Note that this speed does not affect the dispersion of sample). The averaged concentration distribution is dispersed, and the peak value decreases with time due to molecular diffusion. The difference between 2-D and 3-D simulation data here is attributed to the difference of the cross-sectional shape. Such a difference does not exist if the cross section is rectangular because the uniformity of sample species distribution in the z coordinate will not be perturbed in the rectangular geometry. However, with a non-rectangular cross section, like the isotropically-etched one, the non-uniform channel depth breaks the uniformity of the sample distribution in the z coordinate, resulting in the lateral diffusion pattern of the 3-D case deviating from the 2-D case. The variation of the lateral diffusion pattern further changes the dispersion of a sample plug in the longitudinal direction. The initial distribution of sample concentration of the 3-D case is close to that of the 2-D case but, as the dispersion proceeds, the 3-D peak value deviates from the 2-D peak value. The biggest difference (the 2-D value was 3.9% lower) between these two values occurs within 1 sec. As the time passes, the 3-D sample distribution gets closer to that of the 2-D case. In other words, the 3-D geometry effect becomes less significant as the sample plug becomes more uniform in the lateral direction and the sample band increases with time. The result shows that the dispersion of the sample plug during electroosmotic migration in a straight channel is influenced by the geometry when the initial sample plug has laterally non-uniform distribution.

Numerical Inaccuracy Due to Sharp Corners at the Intersection

Previous simulations (4,6,12) have often used geometries containing sharp corners at the intersection probably due to the convenience of generating structured meshes. In traditional fluid dynamics problems with a no-slip boundary condition, a sharp corner does not cause a problem in obtaining the solution because the zero velocity at the wall prevents discontinuous variation of flow velocity. However, since the Helmholtz-Smoluchowski slip flow velocity is adopted for the boundary condition, discontinuous variation of flow velocity at the sharp corner can arise. This discontinuous variation of flow velocity brings an infinite velocity gradient term in the Navier-Stokes equation. This singularity issue does not occur if the no-slip boundary condition is adopted as in references (5,7–8). However, in the current application where a slip boundary condition is adopted, the singularity at the sharp corners may bring numerical inaccuracy. The numerical inaccuracy induced by the sharp edges was investigated by looking at the effect of mesh size near the sharp corners. The simulation case was a 2-D channel with W = 90 μm and a narrow loading method. Figure 9 (a) shows that the size of meshes near the sharp corner significantly affects the injected sample amount. As the size decreases even down to 20 nm, the injection volume keeps on varying, indicating that the mesh independence is not achieved even with such a small mesh size. The variation in the injection volume becomes even more significant at small mesh sizes. For the filleted case, the parameter remains constant with the mesh size below 0.5 μm, indicating the mesh independence. As the mesh size is reduced in the sharp corner geometry, the injected sample amount for the sharp corner case approaches the value

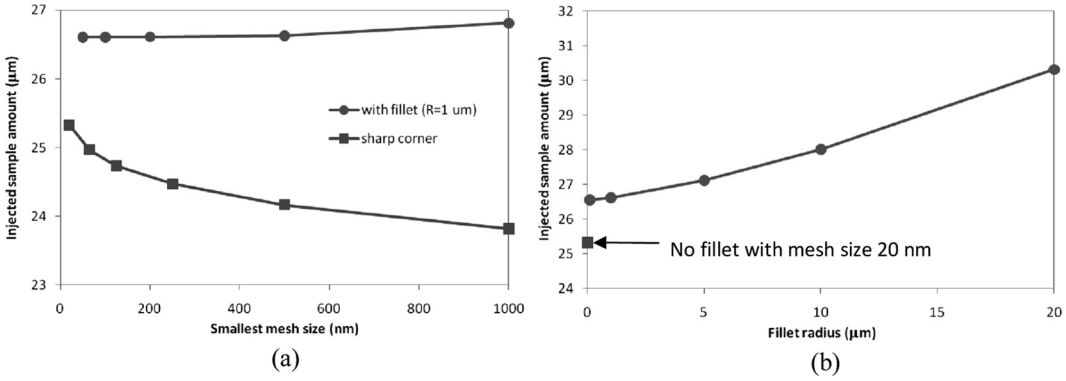

FIG. 9. The effect of (a) mesh size and (b) fillet radius on injection amount.

for the filleted case. This implies that the solution of the filleted geometry case is more accurate. The effect of fillet radius on the injected sample amount is shown in Fig. 9(b). The injected sample volume increases with the fillet radius. However, as the fillet size decreases below 1 μm, the injected sample amount approaches a constant value. The present study shows that the small radius fillet at the corners does not significantly change the performance of the device while it relieves the numerical inaccuracy otherwise developed by singularity related with sharp corners.

CONCLUSIONS

We investigated the 3-D characteristics of the loading and dispensing of sample species during electroosmotic pinched injection in microchip capillary electrophoresis systems that have non-rectangular cross sections. An isotropically-etched channel resulted in a vertically non-uniform sample plug in the loading stage. The cross-sectional sample profile is distorted like a "V" shape or a "Λ" shape depending on the sample loading mode (narrow or wide sample) due to the 3-D non-rectangular geometry of the channel. In the sample injection simulation, the 3-D simulation data showed a clear difference from 2-D simulation data. 2-D simulations employing the top and bottom widths resulted in $3 \sim 10\%$ and $28 \sim 40\%$ errors in injection qualties, respectively. Instead, it was observed that the 2-D simulation data using the width calculated from the equivalent cross-sectional area of the 3-D channel show good agreement with the 3-D simulation data (less than 3% error). This observation gives a guideline as to what width should be selected for a simulation on a pinched injection system when the computer capability limits only to 2-D simulation. As the channel height decreases while the channel width remains fixed, it was found that the 3-D effects decrease and the 3-D results approach the 2-D results. The dispersion of a sample plug during electroosmotic migration in a straight channel is also influenced by the geometry when the initial sample plug has laterally non-uniform distribution. Thus, for an accurate simulation of injection and migration of a sample in a pinched injection device, 3-D simulations provide added insights to the flow field and sample dispersion.

REFERENCES

1. Probstein. (1994) *Physicochemical Hydrodynamics: An Introduction*; Wiley-Interscience.
2. Ghosal, S. (2004) Fluid mechanics of electroosmotic flow and its effect on band broadening in capillary electrophoresis. *Electrophoresis*, 25: 214.
3. Dill, K.A.; Bromberg, S. (2002) *Molecular Driving Forces: Statistical Thermodynamics in Chemistry & Biologys*; Garland Science.
4. Ermakov, S.V.; Jacobson, S.C.; Ramsey, J.M. (1998) Computer simulations of electrokinetic transport in microfabricated channel structures. *Anal. chem.*, 70: 4494.
5. Tsai, C.-H.; Yang, R.-J.; Tai, C.-H.; Fu, L.-M. (2005) Numerical simulation of electrokinetic injection techniques in capillary electrophoresis microchips. *Electrophoresis*, 26: 674.
6. Ermakov, S.V.; Jacobson, S.C.; Ramsey, J.M. (2000) Computer simulations of electrokinetic injection techniques in microfluidic devices. *Anal. Chem.*, 72: 3512.
7. Fu, L.M.; Yang, R.J.; Lee, G.B.; Liu, H.H. (2002) Electrokinetic injection techniques in microfluidic chips. *Anal. Chem.*, 74: 5084.
8. Fu, L.-M.; Lin, C.-H. (2003) Numerical Analysis and experimental estimation of a low-leakage injection technique for capillary electrophoresis. *Anal. Chem.*, 75: 5790.
9. Jorgenson, J.W.; Lukacs, K.D. (1983) Capillary zone electrophoresis. *Science*, 222: 266.
10. Dose, E.V.; Guiochon, G.A. (1991) High-resolution modeling of capillary zone electrophoresis and isotachophoresis. *Anal. Chem.*, 63: 1063.
11. Bercovici, M.; Lele, S.K.; Santiago, J.G. (2009) Open source simulation tool for electrophoretic stacking, focusing, and separation. *J. Chromatography A.*, 1216: 1008.
12. Patankar, N.A.; Hu, H.H. (1998) Numerical simulation of electroosmotic flow. *Anal. Chem.*, 70: 1870.
13. Cummings, E.B.; Griffiths, S.K.; Nilson, R.H.; Paul, P.H. (2000) Conditions for similitude between the fluid velocity and electric field in electroosmotic flow. *Anal. Chem.*, 72: 2526.
14. Jacobson, S.C.; Hergenroder, R.; Koutny, L.B.; Warmack, R.J.; Ramsey, J.M. (1994) Effects of injection shemes and column geometry on the performance of microchip electrophoresis devices. *Anal. Chem.*, 66: 1107.

15. Kim, M.-S.; Cho, S.I.; Lee, K.-N.; Kim, Y.-K. (2005) Fabrication of microchip electrophoresis devices and effects of channel surface properties on separation efficiency. *Sensors and Actuators B*, 107: 818.
16. Kirby, B.J.; Hasselbrink, E.F. (2004) Zeta potential of microfluidic substrates: 1. Theory, experimental techniques, and effects on separations. *Electrophoresis*, 25: 187.
17. Hu, Y.; Werner, C.; Li, D. (2003) Electrokinetic transport through rough microchannels. *Anal. Chem.*, 75: 5747.
18. Young, M.E.; Carroad, P.A.; Bell, R.L. (1980) Estimation of diffusion coefficients of proteins. *Biotechnology and Bioengineering*, 22: 947.
19. Chae, K.S.; Lenhoff, A.M. (2006) Computation of the electrophoretic mobility of proteins. *Biophysical Journal*, 68: 1120.
20. Datta, S.; Ghosal, S.; Patankar, N. (2006) Electroosmotic flow in a rectangular channel with variable wall zeta-potential: Comparison of numerical simulation with asymptotic theory. *Electrophoresis*, 27: 611.
21. Yang, R.-J.; Fu, L.-M.; Lin, Y.-C. (2001) Electroosmotic flow in microchannels. *J. Colloid Interface Sci.*, 239: 98.
22. Chang, C.-C.; Yang, R.-J. (2004) Computational analysis of electrokinetically driven flow mixing in microchannels with patterned blocks. *J. Micromech. Microeng*, 14: 550.
23. Fu, L.-M.; Yang, R.-J.; Lin, C.-H.; Chien, Y.-S. (2005) A novel microfluidic mixer utilizing electrokinetic driving forces under low switching frequency. *Electrophoresis*, 5: 1814.
24. Jacobson, S.C.; Ramsey, J.M. (1997) Electrokinetic focusing in microfabricated channel structures. *Anal. Chem.*, 69: 3212.